Front. Earth Sci. 2016, 10(1): 108–116
DOI 10.1007/s11707-015-0500-0

RESEARCH ARTICLE

Difference of brightness temperatures between 19.35 GHz and 37.0 GHz in CHANG'E-1 MRM: implications for the burial of shallow bedrock at lunar low latitude

Wen YU[1,2], Xiongyao LI (✉)[1], Guangfei WEI[1,2], Shijie WANG[1]

1 Lunar and Planetary Science Research Center, Institute of Geochemistry, Chinese Academy of Sciences, Guiyang 550002, China
2 University of Chinese Academy of Sciences, Beijing 100039, China

Abstract Indications of buried lunar bedrock may help us to understand the tectonic evolution of the Moon and provide some clues for formation of lunar regolith. So far, the information on distribution and burial depth of lunar bedrock is far from sufficient. Due to good penetration ability, microwave radiation can be a potential tool to ameliorate this problem. Here, a novel method to estimate the burial depth of lunar bedrock is presented using microwave data from Chang'E-1 (CE-1) lunar satellite. The method is based on the spatial variation of differences in brightness temperatures between 19.35 GHz and 37.0 GHz (ΔTB). Large differences are found in some regions, such as the southwest edge of Oceanus Procellarum, the area between Mare Tranquillitatis and Mare Nectaris, and the highland east of Mare Smythii. Interestingly, a large change of elevation is found in the corresponding region, which might imply a shallow burial depth of lunar bedrock. To verify this deduction, a theoretical model is derived to calculate the ΔTB. Results show that ΔTB varies from 12.7 K to 15 K when the burial depth of bedrock changes from 1 m to 0.5 m in the equatorial region. Based on the available data at low lunar latitude (30°N–30°S), it is thus inferred that the southwest edge of Oceanus Procellarum, the area between Mare Tranquillitatis and Mare Nectaris, the highland located east of Mare Smythii, the edge of Pasteur and Chaplygin are the areas with shallow bedrock, the burial depth is estimated between 0.5 m and 1 m.

Keywords moon, CE-1, brightness temperature, bedrock, burial depth

1 Introduction

After billions of years of volcanism and high-velocity impacts by numerous meteoroids, most of the lunar bedrock is covered by a layer of regolith. The burial depth of bedrock is not uniform, which might be due to different evolutionary processes during the late period (Heiken et al., 1991). Determination of burial depth of bedrock can help us to understand the formation of regolith, impact process and relative age of the lunar surface (Oberbeck and Quaide, 1968; Wilhelms and McCauley, 1971; Bart et al., 2011).

Burial depths of lunar bedrock have been investigated by direct and indirect explorations. The former includes seismic studies (Watkins and Kovach, 1973; Cooper et al., 1974; Nakamura et al., 1975) and electromagnetic multi-frequency probing (Strangway et al., 1975). A burial depth of about 7 m at the Apollo 17 landing site is deduced from a sharp change in dielectric properties, based on a study of electromagnetic multi-frequency probing with 32 MHz and 16 MHz made at these sites (Strangway et al., 1975). Similar results are obtained from the Apollo 17 seismic profiling experiment, which suggested the transition zone from soil to rock is about 8.5 m below the surface (Olhoeft and Strangway, 1975). On the other hand, indirect explorations which are mainly based on morphological techniques (Oberbeck and Quaide, 1968; Quaide and Oberbeck, 1968; Shoemaker et al., 1969), radar, and microwave radiometer techniques (Shkuratov and Bondarenko, 2001; Fa and Jin, 2007, 2010) show a great potential to reveal the burial depth of bedrock. Based on the radar data, Shkuratov and Bondarenko (2001) estimates the regolith thickness on lunar highland ranges from 1.0 m to 18.0 m and from 1.5 m to 10.0 m on lunar mare. More recently, similar results were obtained by Fa and Jin (2010) by interpreting microwave radiometer data. However, most

Received June 5, 2014; accepted October 21, 2014

E-mail: lixiongyao@vip.skleg.cn

of the above studies using radar and microwave radiometer detection focused on the areas with thick regolith and paid little attention to the areas with thin regolith (0.5–1 m). Determination of the areas with shallow bedrock is helpful to interpret radar data and design future exploration.

In recent years, successive launches of Chang'E-1 (2007), Chang'E-2 (2010) and Chang'E-3 (2013) marked the beginning of a new era in Chinese lunar research. Chang'E-1(CE-1) was equipped with a four-frequency-channel MRM (Microwave Radiometer) for measuring the microwave emission of the Moon from a 200 km orbit. During 16 months of monitoring, global brightness temperature data spanning lunar day and night were obtained. Some primary results pertaining to regolith distribution have been reported (Jiang and Wang, 2008; Jiang et al., 2009; Jiang and Jin, 2010). In this study, we present a novel way to investigate distribution and burial depth of shallow bedrock. The brightness temperature difference, or difference in penetrated depth, between two high-frequency channels, 19.35 GHz and 37.0 GHz, defined as $\Delta TB = TB_{19.35} - TB_{37.0,}$ is discussed in relation to burial depth.

2 Data

There are four channels in the CE-1 MRM, i.e., 3.0 GHz, 7.8 GHz, 19.35 GHz, and 37.0 GHz. According to the microwave transmission properties, the penetration depths of the four channels in CE-1 MRM are about 5 m, 2 m, 1 m, and 0.5 m, respectively (Jiang and Wang, 2008; Li et al., 2010). The spatial resolution is about 35 km for the channels 7.8 GHz, 19.35 GHz, and 37 GHz, and 50 km for 3.0 GHz. The sensitivity of the MRM is about 0.5 K (Jiang and Wang, 2008; Jiang et al., 2009; Zheng et al., 2012). In this study, the brightness temperature data from the 19.35 GHz and 37 GHz from CE-1 MRM channels are used.

Brightness temperatures (TB) of the two high-frequency channels reveal the heat radiation characteristics of the shallow lunar subsurface. Therefore, the differences between the brightness temperatures of two channels can be used to study the shallow structural properties of the lunar surface. Because the spatial resolutions (35 km) and the orientation of the antenna are the same for the two channels, the areas monitored by the two channels are identical at any time. Thus, difference of brightness temperatures (ΔTB) between two channels reflects the different vertical properties. Topography may have an impact on $TB_{37.0}$ and $TB_{19.35}$. But ΔTB denotes the difference between two brightness temperatures, so we think the impact of topography on ΔTB is negligible. Observation time is another factor that can influence $TB_{37.0}$ and $TB_{19.35}$. For the same area, variable solar radiation with time can change the temperature of the lunar surface and the contribution of lunar surface to TB, which could change ΔTB. To minimize the effect of observation time and surface temperature, data in a smaller time range during nighttime are preferred when estimating the burial depth of bedrock. To evaluate the time effect on ΔTB, data from different times at several typical areas are examined (Fig. 1). Figure 2 shows the influence of time interval (Δt) on the fluctuation of ΔTB (δ). It can be seen that, when the range of observation times is within 20 min, the change of ΔTB is less than 0.5 K, close to the radiometric sensitivity of the two channels of the MRM. Therefore, in this study, the TB data from high-frequency channels within 20 min near lunar midnight (00:20–00:40 and 01:00–01:20) during two monitoring periods (November 27, 2007–February 4, 2008 and May 15, 2008–July 28, 2008) are selected for discussing the distribution and burial depth of bedrock at low lunar latitude. (30°N–30°S).

3 Results and discussion

Figures 3 and 4 show spatial variation of ΔTB at lunar low latitude. The largest ΔTB can be found at the southwest edge of Oceanus Procellarum, the area between Mare Tranquillitatis and Mare Nectaris and the eastern highland of Mare Smythii. In these regions, ΔTB is usually larger than 12.7 K and the maximum is close to 14 K.

According to the analysis above, while the observation times of selected data are within 20 min around the midnight, the time effect on ΔTB is less than 0.5 K. But calculated ΔTB values ranges from 2 K to 14 K in some areas. Thus, we think the effect of observation time on ΔTB is insignificant. Such large variation in ΔTB values in low lunar latitudes should be attributed to another reason. The effect of topography on ΔTB is also excluded since it affects $TB_{37.0}$ and $TB_{19.35}$ simultaneously. Thus, the large variation in ΔTB values as shown in Figs. 3 and 4 might be caused by significant difference of vertical structure, e.g., the burial depth of bedrock.

To examine this deduction, the geomorphology of the regions which have large ΔTB values is investigated using the LOLA DEM data. In the contour maps (Figs. 5–8), the areas with large ΔTB values are always accompanied by dense contours, indicating a large change in elevation and steep slope in these areas. More specifically, the regions with large ΔTB values are usually located in the transition zone between a negative landform and a positive landform.

To detail the characteristics of topography at special regions with large ΔTB, the eastern highland of Mare Smythii (circle marked with A and B in Figs. 3 and 7) and Chaplygin crater (circle marked with C in Figs. 3 and 8) are further analyzed. Both region A and B are located at the steep sides of the crater (Fig. 7). The elevation differences of these areas are 4,319 m and 3,132 m, respectively. And region C also shows a large elevation difference with 3,044 m. Due to large elevation difference, it is difficult for regolith to accumulate during the later impact of meteoroid

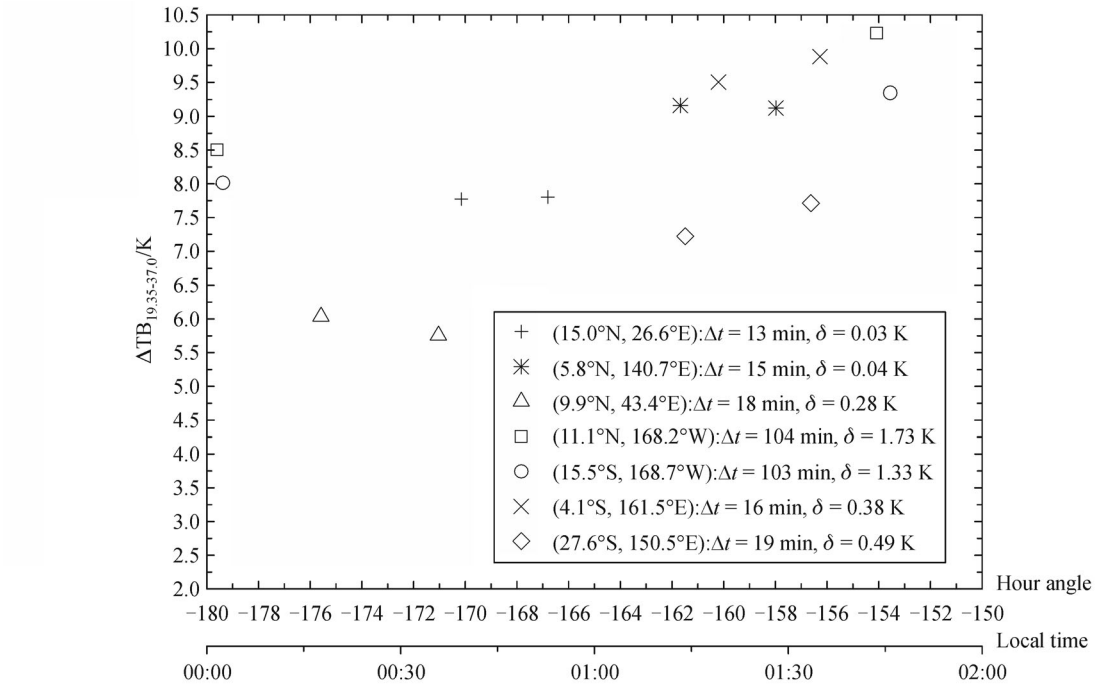

Fig. 1 ΔTB changes with time around the lunar midnight. The UTC time of data is transformed to hour angle and local time by the method proposed by Chan et al. (2010).

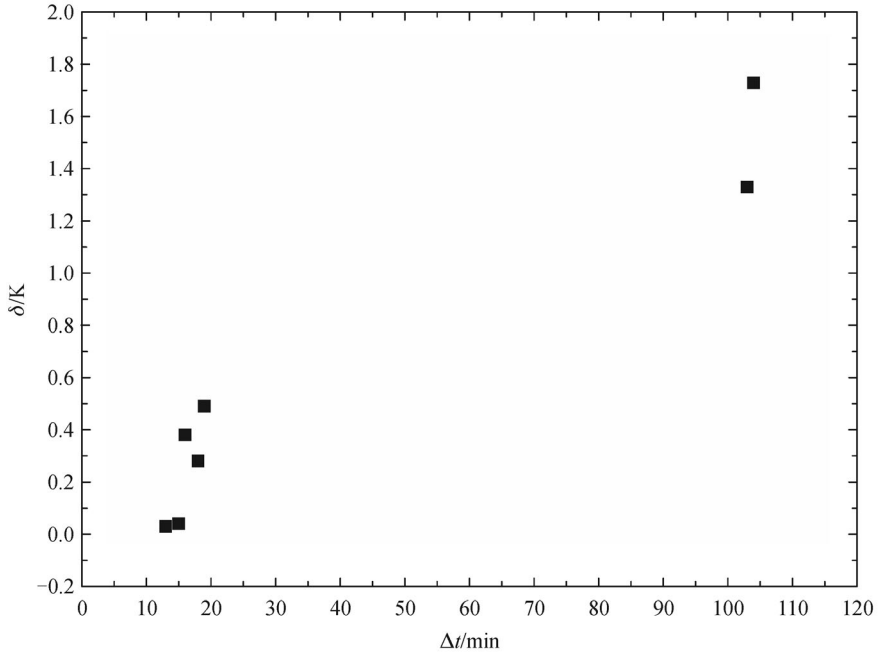

Fig. 2 The fluctuation of ΔTB (δ) as a function of time difference (Δt). The maxima of δ are 1.73 K and 0.49 K when Δt is 104 min and 20 min, respectively.

(Heiken et al., 1991; Bandfield et al., 2011). Reasonably, the burial depth of bedrock is relatively shallow in these regions and shows a correlation with the large ΔTB.

To discuss the relationship between burial depth of bedrock and ΔTB, Aristarchus, Copernicus and Bullialdus Crater (circle marked with D–F in Fig. 4, respectively) are investigated. After analyzing weathering degree, rock concentration and regolith thickness of large craters,

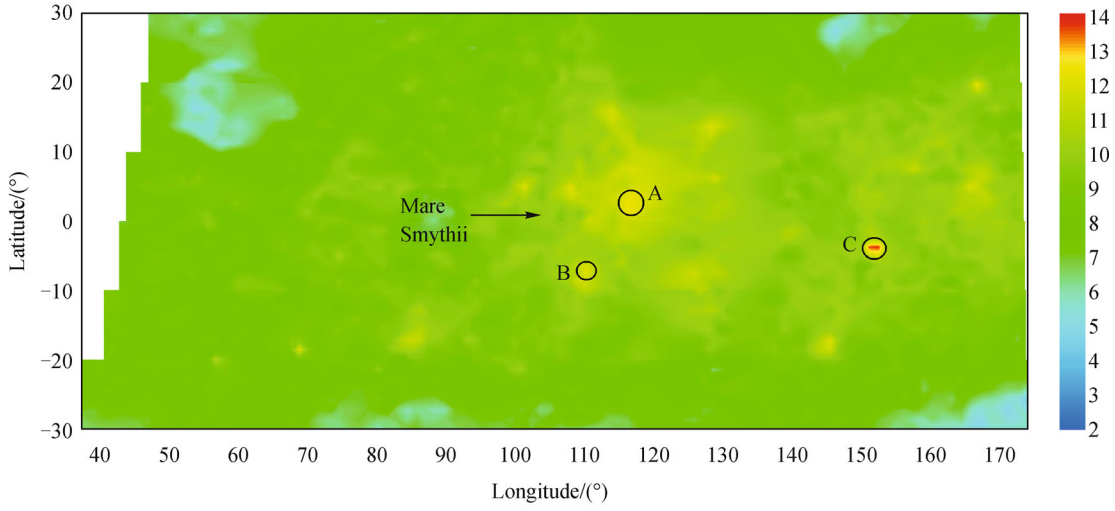

Fig. 3 Map of ΔTB map based on the CE-1's MRM data measured at 01:00 to 01:20 (November 27, 2007 – February 4, 2008 and May 15, 2008 – July 28, 2008). The white color denotes no data available there. The regions characterized by large ΔTB are mainly distributed in the eastern highlands of Mare Smythii. Three typical regions with significant differences in brightness temperatures are marked by circles A–C.

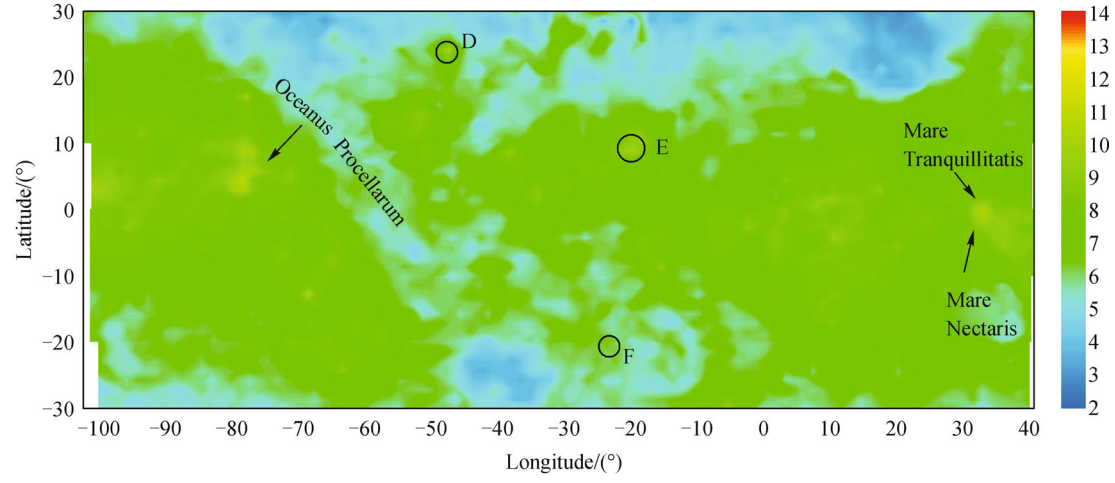

Fig. 4 Map of ΔTB map based on the CE-1's MRM data measured at 00:20 to 00:40 (November 27, 2007 – February 4, 2008 and May 15, 2008 – July 28, 2008). The white color denotes no data available there. Generally, the regions characterized by large ΔTB are the southwest edge of Oceanus Procellarum, and the area between Mare Tranquillitatis and Mare Nectaris. The areas marked by circles D–F on the map are Aristarchus, Copernicus and Bullialdus craters respectively.

Bandfield et al. (2011) concluded that regolith thickness is negatively correlated to rock concentration in craters, i.e., high rock concentration often comes with thin regolith thickness and shallow bedrock. According to the rock concentrations given by Bandfield et al. (2011), Aristarchus Crater with the highest rock concentration has the shallowest bedrock while Bullialdus Crater has the deepest (Fig. 9). In addition, the ages of these craters can also provide some information on the burial depth of bedrock. Usually, accumulation of regolith is relatively limited and bedrock burial is shallow in young craters because of the weak weathering degree (Mendell, 1976). Among the three craters, Aristarchus Crater is the youngest one while Bullialdus Crater is the oldest (Neukum and König, 1976). Thus, the same conclusion can be reached that the bedrocks in Aristarchus Crater and Bullialdus Crater are the shallowest and deepest respectively among the three craters. With the analysis of CE-1 MRM data, ΔTB of Aristarchus, Copernicus and Bullialdus are 11.2 K, 10.3 K and 6.6 K, respectively. Thus it is obvious that ΔTB values show an opposite trend with burial depths of bedrock at the three craters. Aristarchus Crater with shallow bedrock shows the largest ΔTB while Bullialdus Crater is the opposite case.

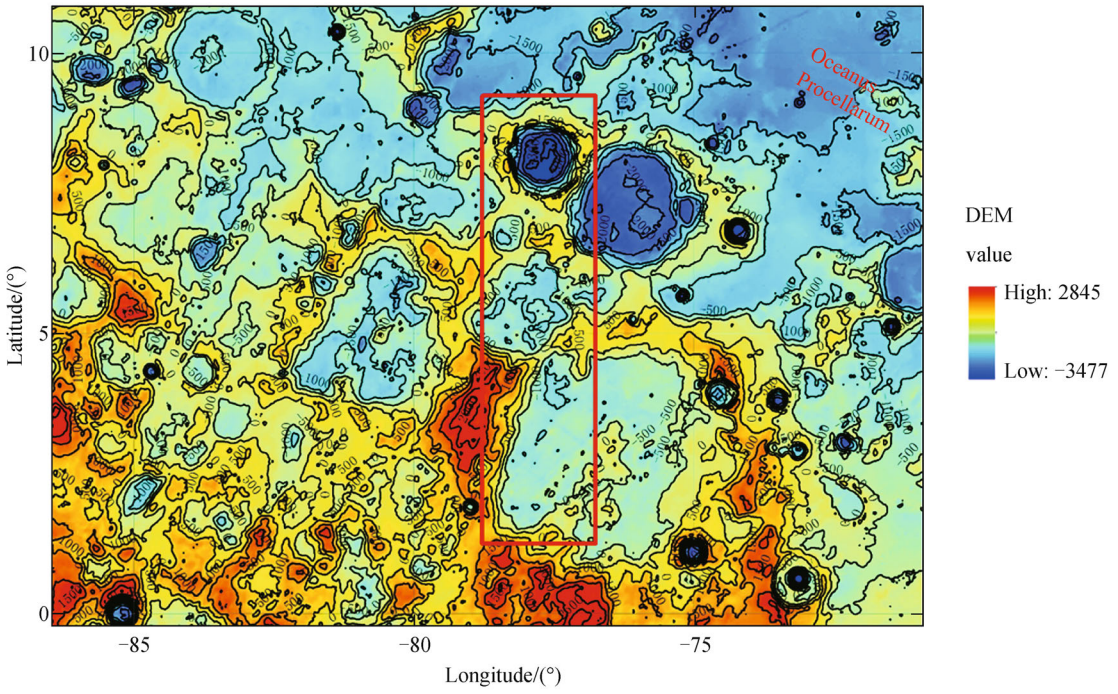

Fig. 5 Contour map of the southwest edge of Oceanus Procellarum using LOLA elevation data. The elevation ranges from −3,477 m to 2,845 m in the area (red rectangle).

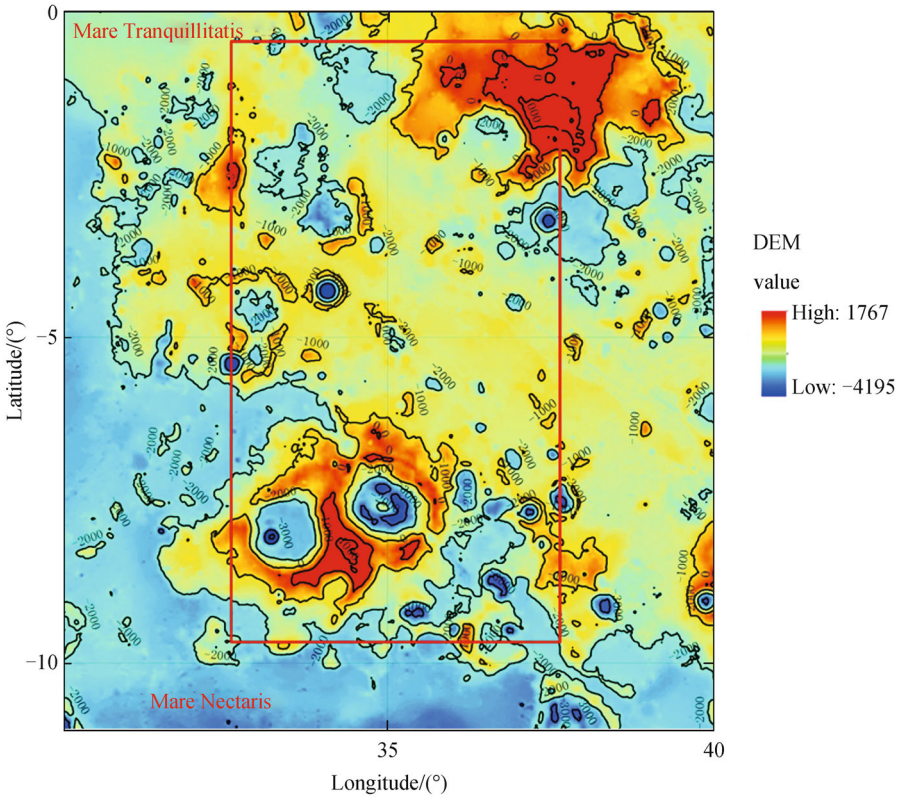

Fig. 6 Contour map of the area between Mare Tranquillitatis and Mare Nectaris using LOLA elevation data. The elevation ranges from –4,195 m to 1,767 m in the area (red rectangle).

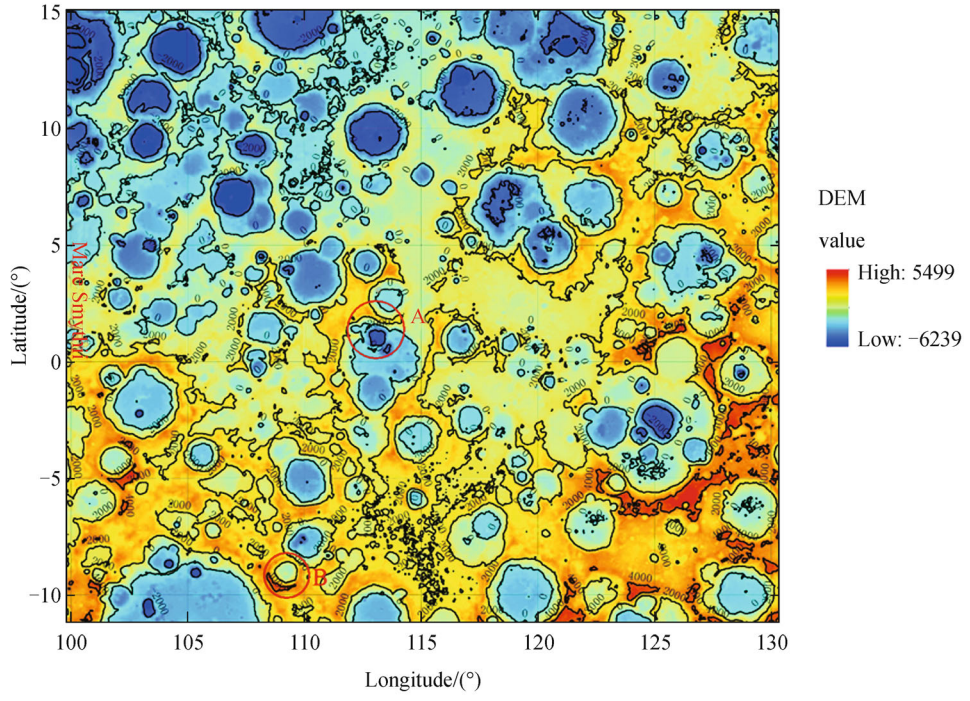

Fig. 7 Contour map of the eastern highlands of Mare Smythii using LOLA elevation data. The areas marked by circles A and B correspond to the areas with large ΔTB in Fig. 3. The elevation differences of areas A and B are 4,319 m and 3,132 m respectively.

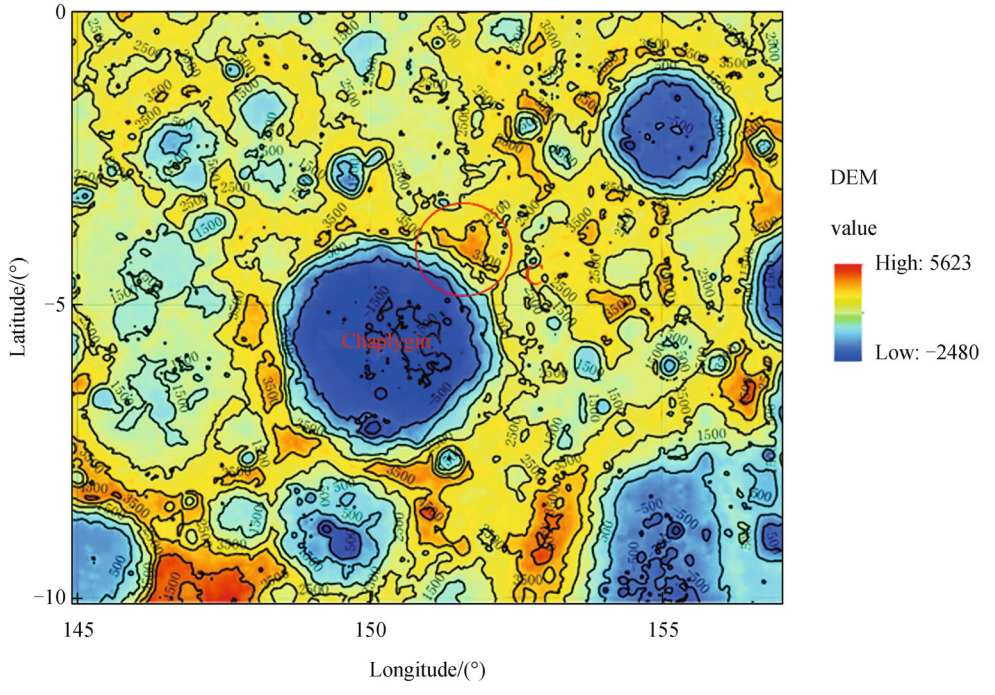

Fig. 8 Contour map of Chaplygin crater using LOLA elevation data. The area marked by circle C corresponds to the area C with high ΔTB value in Fig. 3. The elevation difference of area C is ~3,000 m.

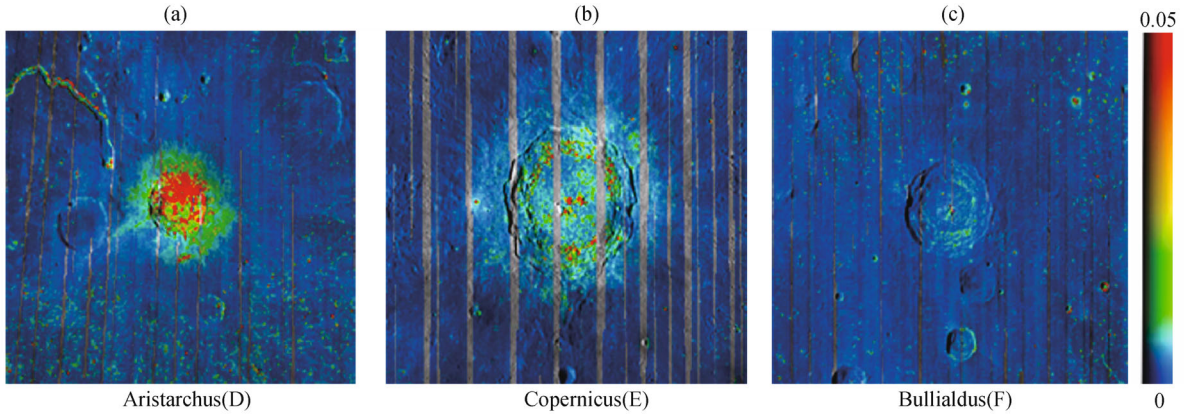

Fig. 9 Rock concentration maps of Aristarchus, Copernicus and Bullialdus craters from Bandfield et al. (2011). (a), (b) and (c) correspond to the areas marked by circles D, E and F respectively in Fig. 4.

As shown above, large ΔTB has the potential to be an indicator of shallow burial depth of bedrock. According to the penetrated depths of 19.35 GHz and 37.0 GHz channels, ΔTB is mainly controlled by the properties of the subsurface layer from 0.5 m to 1 m. When bedrock is buried deeper than 1 m, this layer is full of regolith. When depth to bedrock is less than 1 m, there is some bedrock in this layer. Different structures and properties of this layer might lead to distinct ΔTB values. Based on the theory of microwave radiative transfer, Jin and Fa (2011) proposed a three-layer model to simulate TB theoretically. In their model, the temperature of top layer is considered to be constant, which however is not appropriate since the temperature gradient is very large in the first two centimeters from the top (Vasavada et al., 2012). Vasavada et al. (1999) used a two-layer model to calculate the temperatures at different depths. Their data show that at depths greater than 20 cm temperature remains fairly constant. Thus, in our study, the lunar regolith from the top to 20 cm is regarded as the first layer, where temperature changes significantly. The second layer is the lunar regolith layer from 20 cm to the boundary between regolith and bedrock. The third layer is bedrock. The temperatures in the latter two layers are assumed to be constant. Thus, the equation is given as follows,

$$\begin{aligned}\mathrm{TB} =&(1-r_{01})\left[k_{a1}\int_0^{d_1} T_1(z)\mathrm{e}^{-k_{a1}z}\mathrm{d}z + r_{12}\mathrm{e}^{-k_{a1}d_1}k_{a1}\int_0^{d_1} T_1(z)\mathrm{e}^{-k_{a1}(d_1-z)}\mathrm{d}z\right]\\ &+(1-r_{01})(1-r_{12})(1-\mathrm{e}^{-k_{a2}d_2})(1+r_{23}\mathrm{e}^{-k_{a2}d_2})\mathrm{e}^{-k_{a1}d_1}T_2\\ &+(1-r_{01})(1-r_{12})(1-r_{23})\mathrm{e}^{-k_{a1}d_1}\mathrm{e}^{-k_{a2}d_2}T_3,\end{aligned} \tag{1}$$

where, d_1 is the thickness of the first layer and equal to 0.2 m; d_2 is the thickness of second layer which is variable; $T_1(z)$, T_2 and T_3 are the physical temperatures of the three layers, respectively; z is the depth from the top in the first layer. Definitions of all the other parameters in Eq. (1) are referred in the study of Jin and Fa (2011). According to Fa and Jin (2007), $T_2 = T_3 = 255$ K are used to calculate the TB. The mean dielectric constant of lunar rock equal to $6.84 + 0.342i$ measured at several Apollo landing sites (Heiken et al., 1991) is used in this study. Dielectric constant of lunar regolith is a function of density (ρ) and content (S) of FeO + TiO_2 (Heiken et al., 1991). And ρ changes with depth while S can be calculated with the data of Clementine (Fa and Jin, 2007). In Eq. (1), $T_1(z)$ can be calculated from the following exponential equation (Vasavada et al., 1999),

$$T_1(z) = Ae^{-\beta z} + B, \tag{2}$$

when $z = 0$ and $z = d_1 = 0.2$ m,

$$T_1(0) = A + B, \tag{3}$$

$$T_1(0.2) = A\mathrm{e}^{-0.2\beta} + B = T_2 = T_3. \tag{4}$$

Values of $T_1(0)$ at different latitudes are listed in Table 1 (Bandfield et al., 2011). Based on the data from DivRDR (ch7), β can be supposed to be 20. With the parameters mentioned above, the theoretical ΔTB when the bedrock burial depths are 0.5 m and 1 m are given in Table 2 and 3. From the tables, it can be seen that theoretical ΔTB increases slightly with latitude when bedrock burial is shallow. At the equatorial regions, the theoretical ΔTB is ~12.7 K when bedrock burial depth is 1 m, and it is ~15 K

when bedrock burial depth is 0.5 m. According to ΔTB shown in Figs. 3 and 4, it can thus be inferred that the bedrock burial depths are between 0.5 m and 1 m in some regions of high ΔTB values, such as the southwest edge of Oceanus Procellarum, the southern edge of Mare Tranquillitatis, the eastern highlands of Mare Smythii, and the edges of Pasteur and Chaplygin carters. Most of lunar bedrock is burial deeper than 1 m at low latitude (Fig. 10).

4 Conclusions

The microwave data obtained by CE-1' MRM provide an opportunity to investigate the burial depth of lunar bedrock. To minimize the effect of measurement time (or solar radiation) on ΔTB, data close to midnight (00:20–00:40 and 01:00–01:20) are chosen. Based on the spatial variation in ΔTB values, the southwest edge of Oceanus Procellarum, the area between Mare Tranquillitatis and Mare Nectaris, and the eastern highland of Mare Smythii show large ΔTB values which are generally greater than 12.7 K, and the maximum is close to 14 K. Contour maps of these areas show that all of them are in the transition zone between a negative landform and a positive landform where elevation changes rapidly. That might indicate a shallow burial depth of bedrock in these areas. Based on theoretical calculations, ΔTB ranges from 12.7 K to 15 K when the burial depth of bedrock is between 0.5 m and 1 m at the equatorial regions. With these results, the burial depth of bedrock in the southwest edge of Oceanus Procellarum, the southern edge of Mare Tranquillitatis, the eastern highlands of Mare Smythii, and the edges of Pasteur and Chaplygin crater are estimated to range from 0.5 m to 1 m.

This study presents a new way to study the vertical

Table 1 Initial temperature ($T_1(0)$) at lunar low latitude

Latitude	$T_1(0)$ [a)]		Range
	00:20–00:40	01:00–01:20	
0°	98 K	96 K	10°S–10°N
20°	97 K	95 K	10°N–30°N, 10°S–30°S

a) Temperature data are from Bandfield et al. (2011).

Table 2 Theoretical ΔTB at lunar low latitude from 00:20 to 00:40

Latitude	ΔTB (d^a= 1 m)	ΔTB (d^a= 0.5 m)	Range
0°	12.6 K	14.8 K	10°S–10°N
20°	12.7 K	14.9 K	10°N–30°N, 10°S–30°S

d^a is burial depth of bedrock.

Table 3 Theoretical ΔTB at lunar low latitude from 01:00 to 01:20

Latitude	ΔTB (d^a= 1 m)	ΔTB (d^a= 0.5 m)	Range
0°	12.8 K	14.9 K	10°S–10°N
20°	12.9 K	15 K	10°N–30°N, 10°S–30°S

d^a is burial depth of bedrock.

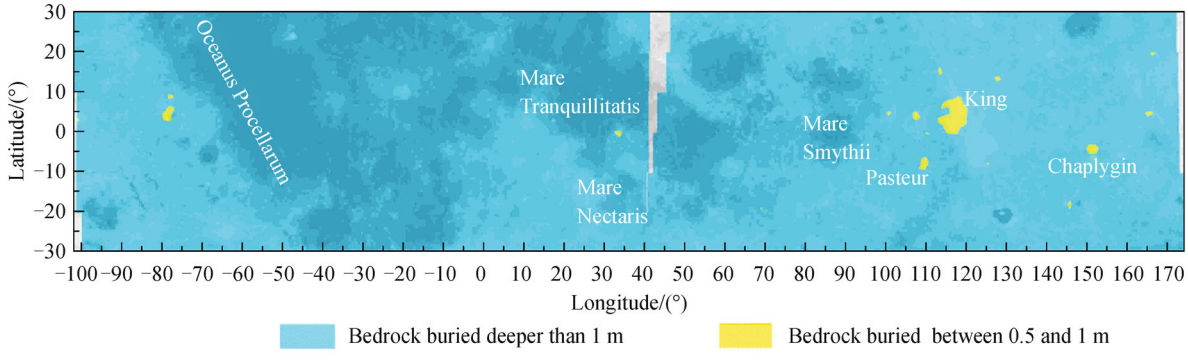

Fig. 10 Burial of bedrock at lunar low latitude (30°S–30°N). The gray denotes no data available there.

structure of the lunar surface and, especially, to estimate the burial depth of bedrock using ΔTB between high-frequency channels. However, it should be noted that calculated ΔTB is an average value in a large area due to the limitation of spatial resolution of MRM. Thus, the inferred burial depth of bedrock also represents an average depth in that area. In the future, high-resolution microwave data will be helpful to determine accurately the distribution of shallow bedrock.

Acknowledgements This study was supported by West Light Foundation of the Chinese Academy of Sciences, Knowledge Innovation Program of the Chinese Academy of Sciences (Lunar Program of Geochemical Institute), and the National Natural Science Foundation of China (Grant Nos. 41373067 and 40803019).

References

Bandfield J L, Ghent R R, Vasavada A R, Paige D A, Lawrence S J, Robinson M S (2011). Lunar surface rock abundance and regolith fines temperatures derived from LRO Diviner Radiometer data. Journal of Geophysical Research: Planets (1991–2012), 116(E12), doi: 10.1029/2011JE003866

Bart G D, Nickerson R D, Lawder M T, Melosh H J (2011). Global survey of lunar regolith depths from LROC images. Icarus, 215(2): 485–490

Chan K L, Tsang K T, Kong B, Zheng Y C (2010). Lunar regolith thermal behavior revealed by Chang'E-1 microwave brightness temperature data. Earth Planet Sci Lett, 295(1–2): 287–291

Cooper M R, Kovach R L, Watkins J S (1974). Lunar near surface structure. Rev Geophys, 12(3): 291–308

Fa W Z, Jin Y Q (2007). Simulation of brightness temperature of lunar surface and inversion of the regolith layer thickness. Journal of Geophysical Research: Planets (1991–2012), 112(E5), doi: 10.1029/2006JE002751

Fa W Z, Jin Y Q (2010). A primary analysis of microwave brightness temperature of lunar surface from Chang'E-1 multi-channel radiometer observation and inversion of regolith layer thickness. Icarus, 207(2): 605–615

Heiken G H, Vaniman DeT, French B M (1991). Lunar Source-Book: A User's Guide to the Moon. London: Cambridge University Press

Jiang J S, Wang Z Z, Zhang X H, Zhang D H, Li Y, Lei L Q, Zhang W G, Cui H Y, Guo W, Li D H, Dong X L, Liu H G (2009). China probe CE-1 unveils world first moon-globe microwave emission map—The microwave moon some exploration results of Chang'E-1 microwave sounder. Remote Sensing Technology and Application, 24(4): 409–422

Jiang J S, Jin Y Q (2010). Selected Papers on Microwave Lunar Exploration in Chinese Chang'E-1 Project. Beijing: Science Press

Jiang J S, Wang Z Z (2008). The microwave moon—Microwave sounding the lunar surface from China lunar orbiter CE-1 satellite. 37th COSPAR meeting, Montreal, Canada

Jin Y Q, Fa W Z (2011). The modeling analysis of microwave emission from stratified media of non-uniform lunar cratered terrain surface for Chinese Chang-E 1 observation. Chin Sci Bull, 56(11): 1165–1171

Li Y, Wang Z Z, Jiang J S (2010). Simulations on the influence of lunar surface temperature profiles on CE-1 lunar microwave sounder brightness temperature. Science China: Earth Sciences, 53(9): 1379–1391

Mendell W W (1976). Degradation of large, period II lunar craters. In: Lunar and Planetary Science Conference Proceedings, 7: 2705–2716

Nakamura Y, Dorman J, Duennebier F, Lammlein D, Latham G (1975). Shallow lunar structure determined from the passive seismic experiment. Moon, 13(1–3): 57–66

Neukum G, König B (1976). Dating of individual lunar craters. In: Lunar and Planetary Science Conference Proceedings, 7: 2867–2881

Oberbeck V R, Quaide W L (1968). Genetic implication of lunar regolith thickness variations. Icarus, 9(1–3): 446–465

Olhoeft G R, Strangway D W (1975). Dielectric properties of the first 100 meters of the Moon. Earth Planet Sci Lett, 24(3): 394–404

Quaide W L, Oberbeck V R (1968). Thickness determinations of the lunar surface layer from lunar impact craters. J Geophys Res, 73(16): 5247–5270

Shkuratov Y G, Bondarenko N V (2001). Regolith layer thickness mapping of the Moon by radar and optical data. Icarus, 149(2): 329–338

Shoemaker E M, Batson R M, Holt E S, Morris H E, Rennilson J J, Whitaker E A (1969). Observations of the lunar regolith and the Earth from the television camera on Surveyor 7. J Geophys Res, 74(25): 6081–6119

Strangway D, Pearce G, Olhoeft G (1977). Magnetic and dielectric properties of lunar samples. In: Promeroy J H, Hubbard N J, eds. The Soviet–American Conference on Cosmochemistry of the Moon and Planets. NASA SP-370, 417–433

Vasavada A R, Bandfield J L, Greenhagen B T, Hayne P O, Siegler M A, Williams J P, Paige D A (2012). Lunar equatorial surface temperatures and regolith properties from the Diviner Lunar Radiometer Experiment. J Geophys Res, 117(E12): E00H18

Vasavada A R, Paige D A, Wood S E (1999). Near surface temperatures on mercury and the moon and the stability of polar ice deposites. Icarus, 141(2): 179–193

Watkins J S, Kovach R L (1973). Seismic investigation of the lunar regolith. Proceedings of the Fourth Lunar Science Conference, 3: , 2561–2574

Wilhelms D E, McCauley J F (1971). Geologic map of the near side of the Moon. U.S. Department of the Interior, U.S. Geological Survey

Zheng Y C, Tsang K T, Chan K L, Zou Y L, Zhang F, Ouyang Z Y (2012). First microwave map of the Moon with Chang'E-1 data: the role of local time in global imaging. Icarus, 219(1): 194–210